HYBRID PARTICLE-IN-CELL SIMULATIONS OF STIMULATED BRILLOUIN SCATTERING INCLUDING ION–ION COLLISIONS

P. W. Rambo

S. C. Wilks

W. L. Kruer

Introduction

Stimulated Brillouin scattering (SBS) is an instability in which intense laser light incident on a target can decay into a scattered light wave and an ion sound wave. The process requires frequency and wave vector matching (i.e., $\omega_0 = \omega_{sc} + \omega_i$ and $\mathbf{k}_0 = \mathbf{k}_{sc} + \mathbf{k}_i$), which corresponds to energy and momentum conservation. Here ω_0 (ω_{sc}) is the frequency of the incident (scattered) light wave; ω_i is the frequency of a sound wave in the plasma; and $\mathbf{k}_0$, $\mathbf{k}_{sc}$, $\mathbf{k}_i$ are the corresponding wave vectors. It is important to understand and control this instability to optimize energy deposition in inertial fusion targets.

Although there has been much progress in characterizing SBS in experiments,[1,2] a better understanding of the nonlinear behavior is clearly needed. The nonlinear behavior of the ion wave is particularly complex. Collisionless particle-in-cell (PIC) simulations[3–7] have emphasized strong distortions in the ion distribution function near the ion wave phase velocity. The damping and dispersion of the driven ion wave are then determined by nonlinear processes, such as trapping, self-consistent tail formation, and mode coupling. It should be emphasized that the distributions are modified quite rapidly even when the driven ion wave has a rather small amplitude. A characteristic time for the ion distribution to distort is $\tau_b = \pi/\omega_b$, where ω_b is the bounce frequency of a resonant ion in the potential trough of the ion wave. Here $\omega_b = (ZeEk_i/M)^{1/2}$, where E is the electric field, k_i the wave number, Z the ion charge state, and M its mass. For even a very small ion wave amplitude corresponding to a fluctuating density $\delta n/n \approx 1\%$, the bounce time is only about 1 ps in typical experiments using 0.35-μm lasers.

It is readily seen that ion–ion collisions can strongly reduce these distortions of the ion distribution function, especially in high-Z plasmas found in laser-irradiated hohlraums. The scattering rate of an ion at the phase velocity [approximated as the sound speed, $C_s \equiv (ZT_e/M)^{1/2}$] is

$$\nu_\perp = \frac{6\sqrt{\pi}}{(ZT_e/T_i)^{3/2}}\tau_i^{-1} \quad , \tag{1}$$

where T_e (T_i) is the electron (ion) temperature and τ_i is the Braginskii ion–ion collision time

$$\tau_i \equiv \frac{3\sqrt{M}\,T_i^{3/2}}{4\sqrt{\pi}\,Z^4 e^4 n_i \lambda_{ii}} \quad . \tag{2}$$

Here, n_i is the ion number density and λ_{ii} is the Coulomb logarithm for ion–ion collisions. The time required for collisions to restore the distribution is determined by the trapping width ($\delta v_{trap} \approx 2\omega_b/k_i$) and $\nu_\perp$:

$$\tau_{detrap} \approx \frac{2}{\nu_\perp}\left(\frac{\delta v_{trap}}{C_s}\right) \approx \frac{4}{\nu_\perp}\left(\frac{\delta n}{n}\right)^{1/2} \quad . \tag{3}$$

These arguments are easily generalized to the case of a plasma composed of a light minority species (α) and a heavy species (β).

In the following example, Be is added to a Au plasma[8] to increase the Landau damping of the ion waves. For an equal mixture Au^{+50}/Be^{+4} plasma, with electron temperature $T_e = 3$ keV, $\delta n/n = 0.05$, electron plasma density $n_e = n_c/4$ (n_c = critical density), and $k_i = 3.5 \times 10^5/\text{cm}^1$ ($\approx 2k_0$ for blue laser light): $\tau_{detrap} \approx \tau_{bounce} \approx 1$ ps. Similar results can be estimated for recent gas bag experiments with Xe/H mixtures.[9]

In addition to countering and/or modifying tail formation in the nonlinear state, ion–ion collisions can inhibit the transport of heated ions from the interaction region. (In collisionless simulations, they simply free-stream away.) The reduced transport enhances the local

ion heating, which can reduce the instability growth. Such an effect will be particularly important on long time scales, when significant energy has been transferred via the driven ion waves.

Hybrid Simulation Model

Hybrid simulations, which model some physical species with particles and others with fluids, have been applied to a wide variety of problems in magnetically confined fusion plasmas and space plasma physics. Typically, the regime of interest is such that the ions are essentially collisionless and require a kinetic treatment, while the electrons may be represented by a fluid. More recently, such simulation models are being applied to laser-generated plasmas.[4–7] Our simulations are performed in one spatial dimension, using a PIC description for the kinetic ions and an isothermal electron fluid at constant temperature T_e. The particle ion velocities and positions are simply advanced by

$$\frac{dx}{dt} = v_x \ , \quad \frac{dv_x}{dt} = \frac{ZeE_x}{M} \ , \tag{4}$$

using the longitudinal electric field $E_x = -\partial\Phi/\partial x$. The electrostatic potential Φ is found from solution of the nonlinear Poisson equation in terms of the total ion charge density and the electron density (n_e) given by a Boltzmann relation,

$$-\partial^2\Phi/\partial x^2 = 4\pi e\left(\Sigma_i Z_i n_i - n_e\right);$$
$$n_e \equiv n_0 \exp\left\{e\left(\Phi - \Phi_{\text{pond}}\right)/T_e\right\} \ . \tag{5}$$

The use of a reduced treatment for the electrons enables efficient simulation of longer time scales; in particular, the restriction of resolving the electron plasma frequency is relaxed. The ponderomotive potential $\Phi_{\text{pond}} = m_e\left\langle u_y^2\right\rangle/2$ is accumulated in time during the explicit advance of the electromagnetic field equations and transverse electron fluid velocity (u_y), which are subcycled in time relative to the ion particle advance. Use of the nonlinear Poisson equation retains the physics of charge separation due to finite-electron Debye length, and hence includes modifications to the ion-acoustic dispersion relation embodied in the linear dispersion relation $\left(w/kC_s\right)^2 = \left(1 + k^2\lambda_{De}^2\right)^{-1}$, where $\lambda_{De} = (4\pi n_e e^2/T_e)^{-1/2}$ is the Debye length.

Although for the parameters considered here the dispersive effect of finite $k\lambda_{De}$ is small, the smoothing achieved is beneficial in reducing numerical heating, a major concern for these high ZT_e/T_i plasmas.[10]

Additionally, we use quadratic splines to interpolate between particles and grid and large numbers of particles per cell, typically 200 to 400 for each ion species. The use of quadratic splines reduces numerical heating approximately an order of magnitude compared to linear interpolation.

Ion–ion collisions between particles are handled using a scheme substantially like that developed by Takizuka and Abe.[11] Particles sharing the same spatial cell are randomly paired up and then undergo a collision irrespective of their positions in the cell. Each collision is kinematically correct, thus ensuring microscopic momentum and energy conservation. For scattering between species α and β, the collision is performed in the center of mass frame for each particle pair with a polar scattering angle picked from a Gaussian distribution of width,

$$\left\langle\theta^2\right\rangle \equiv \frac{8\pi Z_\alpha^2 Z_\beta^2 e^4 \lambda_{\alpha\beta} n_\beta}{m_{\alpha\beta}^2 |\delta\mathbf{v}|^3}\,\delta t \ , \tag{6}$$

where $m_{\alpha\beta} = m_\alpha m_\beta/(m_\alpha + m_\beta)$ is the reduced mass and $\delta\mathbf{v}$ is the relative velocity between each scattering pair. The collisional time period δt is typically equal to the particle advance time step Δt or a small multiple of it. The azimuthal scattering angle is picked uniformly over the interval $[0, 2\pi]$. The postcollision velocity of the particle from species β is given by the kinematic relations. The Coulomb logarithm $\lambda_{\alpha\beta}$ is set to a constant in these simulations and provides a convenient multiplier to vary the collisionality. Extensive tests have verified that this method is equivalent to a Fokker–Planck description of cumulative small-angle Coulomb scattering. In the multispecies simulations performed here, typically only the light–heavy species (α–β) collisions were included. The rate of collisions between light ions (α–α) is typically low enough to ignore, while the heavy–heavy (β–β) collisions also contribute little to wave damping. In fact, failure to properly resolve the short collisional scales for heavy–heavy collisions can artificially enhance the wave damping rate.

Wave Damping

As a simple illustrative example of the relevant physics, we first consider the damping of a finite-amplitude ion wave composed of a mixture of light and heavy ions. The linear damping of such a mixed-species plasma has been discussed by several authors, both with[12,13] and without[14] collisions. Consider the Au/Be plasma previously discussed. We can estimate the ion Landau damping in the absence of collisions to be approximately $\gamma_i \approx 0.07\omega_i$. Figure 1a shows the time history of the electron fluid velocity from a simulation of a single wavelength, initially with amplitude

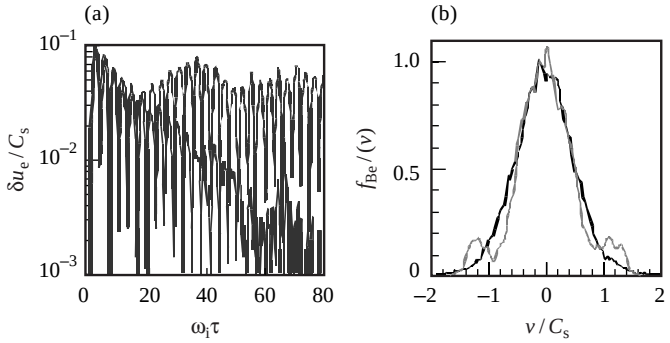

FIGURE 1. Damping of a small-amplitude wave in a Be / Au plasma: (a) time history of electron fluid velocity and (b) velocity distribution of Be ions for collisionless (gray line) and collisional (black line) simulations. (50-00-0898-1711pb01)

perturbation $\delta n/n = 0.05$. (Because the plasma is initialized as a standing wave, the total initial ion density perturbation is the sum of left- and right-going waves, $2\delta n/n = 0.10$). We can clearly see the initial linear decay with $\gamma_i \approx 0.07\omega_i$, followed by a recurrence due to nonlinear trapping; this occurs at time $t \approx 1$ ps $\approx \tau_b$. The ion velocity distribution is presented in Figure 1b, clearly showing the nonlinear distortion near the phase velocity of the ion wave. In contrast, a simulation including ion–ion collisions between the Au and Be particles is also shown, which displays steady linear damping.

It is important to note that the linear damping rate is unaffected by this level of collisions ($\lambda_{\alpha\beta} = 2$). This is consistent with estimates for the amount of damping contributed by frictional and viscous effects caused by collisions, $\gamma_{collision} \approx 5 \times 10^{-3}\ \omega_i << \gamma_{Landau.}$[13] Increasing or decreasing the collisionality by a factor of two was observed to have essentially no effect, either on the linear damping rate or the supression of trapping. Significantly decreasing the collision rate eventually returns to the collisionless result of nonlinear trapping; significantly increasing the collisionality eventually suppresses Landau damping, and the wave damping rate is observed to monotonically decrease with further increases in collisionality. (Much like the situation of a single-ion species,[15] a mixture with reduced ion Landau damping, e.g., $T_e / T_i = 8$, exhibits a maximum in the wave damping for $\nu_{\alpha\beta} \approx \omega_i$, where $\nu_{\alpha\beta}$ is the generalization of Branginskii's collision time for multiple species[13]).

Self-Consistently Driven Ion Waves

We now consider a case with ion waves self-consistently driven by SBS. The system is a finite-length plasma slab composed of the same Au / Be plasma just considered, with laser light (wavelength $\lambda_0 = 0.35$ μm) of intensity $I_0 = 4.0 \times 10^{15}$ W / cm^2, incident from the left-hand side. The plasma slab is composed of an active plasma region (represented by particles) $L = 11$ μm, buffered between fixed ion regions; the fixed ions prevent plasma expansion driven by the ambipolar field at the slab edges, which have linear density ramps to minimize reflection. The density profile is shown in Figure 2a for a collisionless case, illustrating the geometry as well as showing the strong ion wave fluctuations present in this case due to SBS. The time-dependent reflectivity is presented in Figure 2b; note that it reaches a very high level, $R \approx$ 80%. Inspection of the ion velocity phase space shows trapping of resonant ions in the large-amplitude waves, $\delta n/n \approx$ 15–20%. For comparison, an identical case except for ion–ion collisions ($\lambda_{\alpha\beta} = 2$) is also presented that shows a significant decrease in the saturated reflectivity $R < 1$%. For this case, the instability saturates at a much lower level, $\delta n/n \approx$ 2–3%, and although the ion velocity distribution shows strong heating, the slope of the distribution is observed to still be monotonic. We note that a reduction in the reflection is one effect in the right direction, because collisionless simulations have typically predicted too much reflectivity from large regions of plasma.

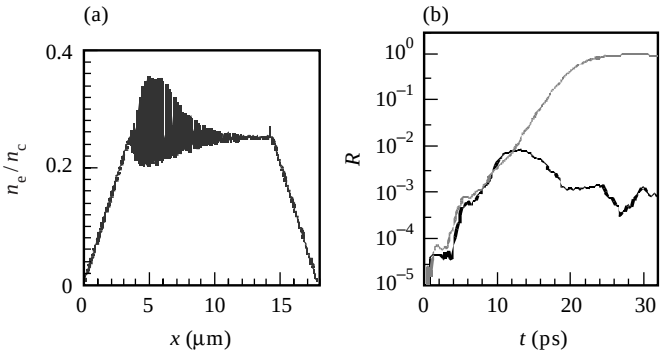

FIGURE 2. Simulations of SBS in a Be / Au plasma: (a) electron density from a collisionless simulation and (b) time-dependent reflectivities from collisionless (gray line) and collisional (black line) simulations. (50-00-0898-1712pb01)

The saturated ion wave amplitude for the collisional case is consistent with our earlier estimates of the level below which collisions can repopulate the resonant region and counteract trapping. The collision rate necessary to maintain wave damping depends on the strength of the instability driving the ion waves. This is illustrated by a set of simulations presented in Figure 3 for a fully ionized CH plasma (1:1, $n_e = n_c / 4$, $T_e = 10T_i = 3$ keV, $L = 22$ μm). In Figure 3a, the time-dependent reflectivity for an incident intensity of $I_0 = 2.7 \times 10^{15}$ W / cm^2 is compared for a collisionless simulation and three collisional runs employing half, nominal, and double

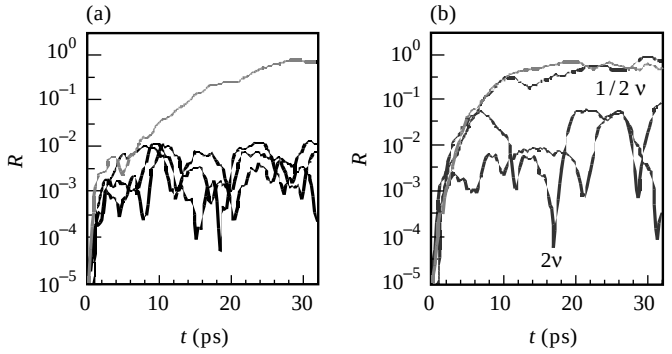

FIGURE 3. Time-dependent SBS reflectivities for CH plasma comparing collisionless (gray line) and collisional (black lines) simulations for intensity (a) $I_0 = 2.7 \times 10^{15}$ W/cm^2 and (b) $I_0 = 3.4 \times 10^{15}$ W/cm^2; three collisional runs employ nominal, half, and double collisionality. (50-00-0898-1713pb01)

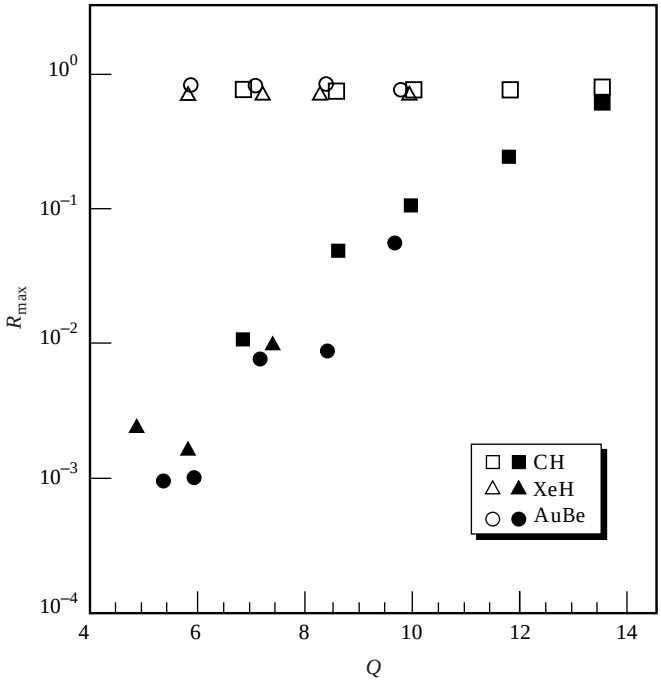

FIGURE 4. Maximum reflectivity observed in simulations of SBS with and without collisions as a function of the linear gain exponent; closed and open symbols are collisional and collisionless results, respectively. (50-00-0898-1725pb01)

collisionality ($\lambda_{\alpha\beta}$ = 2, 4, and 8 respectively); all the collisional runs are similar with peak reflectivity $R \approx 1\%$. A similar insensitivity was found for the Au/Be plasma case previously described. In contrast, increasing the incident pump strength to $I_0 = 3.4 \times 10^{15}$ W/cm^2, as shown in Figure 3b, drives the ion waves strongly enough that the case with collisionality halved now nearly follows the collisionless result. If the collision rate is significantly increased, however, the wave damping is decreased, increasing the linear gain and increasing the reflectivity. An additional simulation at $I_0 = 3.4 \times 10^{15}$ W/cm^2 with collisionality increased by a factor of thirty clearly showed faster instability growth, consistent with the decreased damping ($\gamma_i/\omega_i \approx 0.06$ measured in a linear wave damping test). In spite of this, the saturated reflectivity ($R \approx 10\%$) was still lower than the collisionless result.

A number of self-consistent SBS simulations are summarized in Figure 4, which shows peak reflectivity as a function of the linear gain exponent

$$Q \equiv \frac{\pi}{4}\left(\frac{L}{\lambda_0}\right)\left(\frac{n_e/n_c}{1-n_e/n_c}\right)\left(\frac{v_0}{v_e}\right)^2\left(\frac{\gamma_i}{\omega_i}\right)^{-1}, \qquad (7)$$

where v_0/v_e is the ratio of an electron's quiver velocity in the pump laser field to its thermal velocity. In all the simulations, the electron parameters were $n_e = n_c/4$ and T_e = 3 keV. We see that the collisionless reflectivities are all very large and only weakly dependent on the gain. In contrast, the simulations including ion–ion collisions more nearly follow an exponential gain relationship, $R \approx R_0 \exp(Q)$, until the gain is large enough to drive the ion wave amplitude beyond the level where collisions keep pace with the trapping. In addition to the Au^{+50}/Be^{+4} and C^{+6}/H^+ plasmas, simulations are also shown for a Xe^{+44}/H^+ mixture (1:4, $T_e = 2T_i$, $\lambda_{\alpha\beta} = 2$, L = 11 μm) with similar behavior. This Xe/H plasma differs fundamentally in that the resonant ion wave is the slow mode, with phase velocity smaller than the proton thermal velocity. Simulations of the damping of small amplitude waves determined the damping rates used in Eq. 7 to calculate the linear gain, $\gamma_i/\omega_i \approx 0.10$ for the C/H plasma and $\gamma_i/\omega_i \approx 0.05$ for the Xe/H plasma.

In addition to affecting tail formation, ion–ion collisions can inhibit the transport of heated ions from the interaction region. We illustrate this with a simulation of a single-species plasma, Au^{+50} ($n_e = n_c/4$, $T_e = T_i$ = 3 keV, L = 11 μm). The sound speed $C_s = 2.7 \times 10^7$ cm/s is much larger than the ion thermal velocity $v_i = (T_i/m_i)^{1/2} = 3.8 \times 10^6$ cm/s, so that ion Landau damping is very weak. (In fact, no resonant particles are initially present in the simulation.) Because of the large ratio of sound speed to thermal velocity, collisional damping of the wave is also very small, in spite of the large collision rate $\tau_i\omega_i \approx 0.10$. Thus, the reflectivities from two simulations with and without collisions are initially very similar, as shown in Figure 5a. The driven ion waves are very large, so that collisions are slow to repopulate the tail. Collisions are effective, however, in preventing the heated ions from free-streaming out of the simulation as rapidly as occurs in the collisionless case. Figure 5b shows the mean ion energy $\langle \varepsilon_i \rangle$ as a function of position from the collisional simulation at two different times; although not Maxwellian, the ion distribution is fairly isotropic.

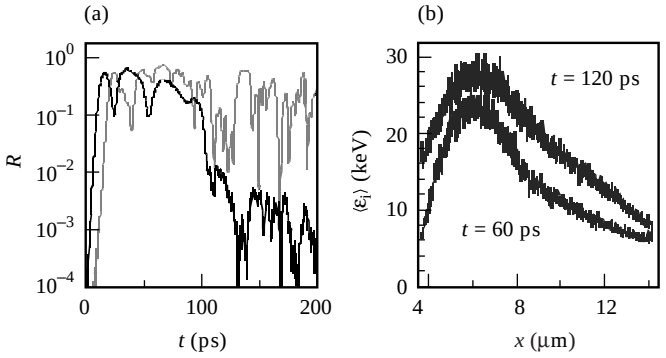

FIGURE 5. Simulations of SBS in a Au plasma showing (a) reflectivities from collisionless (gray line) and collisional (black line) simulations and (b) average ion energy as a function of position from collisional simulation. (50-00-0898-1714pb01)

At late time ($t > 100$ ps), the mean ion energy exceeds 20 keV for much of the simulation region, and the reflectivity is significantly reduced compared to the collisionless run. This decrease in reflectivity can be interpreted as being due to the increase in linear damping of the ion waves. This increase in linear damping may be due to Landau damping from the nonlinearly populated tails, but is also due to increased collisional damping. Assuming a Maxwellian with $T_i = 15 \text{ keV} \approx 2 \langle \varepsilon_i \rangle / 3$, the collisional wave damping[15] is $\gamma_i / \omega_i \approx 0.04$, and the linear gain exponent of the system is reduced to $Q \approx 7$. The late-time reflectivity is consistent with this reduced gain.

Conclusion

In summary, we have shown the important effect that ion–ion collisions can have on SBS. By restoring the nonlinearly distorted distribution function, damping is maintained closer to the linear value, significantly reducing the reflectivity observed in simulations. The fact that damping is maintained close to the linear value for finite-amplitude ion waves is important to the interpretation of recent experiments,[9,16] which have observed an inverse correlation between stimulated Raman scattering and linear ion wave damping, as well as one important justification for reduced descriptions of coupled parametric processes that assume linear damping. Collisions also modify the ion transport and enhance long-term changes in the plasma conditions, which can disrupt SBS. Although not always important, the collisional effects we have identified should be assessed for each application.

Acknowledgments

The authors wish to acknowledge helpful discussions with R. L. Berger, B. Cohen, A. B. Langdon, and B. Lasinski.

Notes and References

1. H. A. Baldis, E. M. Campbell, and W. L. Kruer, *Physics of Laser Plasmas* (North Holland, Amsterdam, 1991) pp. 361–434, and many references therein.
2. B. J. MacGowan et al., *Phys. Plasmas* **3**, 2029 (1996).
3. D. W. Forslund, J. M. Kindel, and E. L. Lindman, *Phys. Rev. Lett.* **30**, 739 (1973).
4. W. L. Kruer, E. J. Valeo, and K. G. Estabrook, *Phys. Rev. Lett*. **35**, 1076 (1975).
5. S. C. Wilks et al., *Phys. Rev. Lett*. **74**, 5048 (1995).
6. B. I. Cohen, B. F. Lasinski, A. B. Langdon, and E. A. Williams, *Phys. Plasmas* **4**, 956 (1997).
7. H. X. Vu, *J. Comput. Phys*. **124**, 417 (1996).
8. R. K. Kirkwood et al., *Phys. Plasmas* **4**, 1800 (1997).
9. R. K. Kirkwood et al., *Phys. Rev. Lett*. **77**, 2706 (1996).
10. P. W. Rambo, *J. Comput. Phys*. **133**, 173 (1997).
11. T. Takizuka and H. Abe, *J. Comput. Phys*. **25**, 205 (1977).
12. E. M. Epperlein, R. W. Short, and A. Simon, *Phys. Rev. E* **49**, 2480 (1994).
13. V. Yu. Bychenkov, W. Rozmus, and V. T. Tikhonchuk, *Phys. Rev. E* **51**, 1400 (1995).
14. H. X. Vu, J. M. Wallace, and B. Bezzerides, *Phys. Plasmas* **1**, 3542 (1994); E.A. Williams et al., *Phys Plasmas* **2**, 129 (1995).
15. C. J. Randall, *Phys. Fluids* **25**, 2231 (1982); M. D. Tracy et al., *Phys. Fluids B* **5**, 1430 (1993).
16. Juan C. Fernández et al., *Phys. Rev. Lett*. **77**, 2702 (1996).